Computer Physics Communications 182 (2011) 1904–1908

Contents lists available at ScienceDirect

Computer Physics Communications

www.elsevier.com/locate/cpc

Light scattering from anisotropic, randomly rough, perfectly conducting surfaces

Ingve Simonsen [a,b,*], Jacob B. Kryvi [a], Alexei A. Maradudin [c], Tamara A. Leskova [c]

[a] Department of Physics, Norwegian University of Science and Technology (NTNU), NO-7491 Trondheim, Norway
[b] Institut des NanoSciences de Paris, Paris, France
[c] Department of Physics and Astronomy and Institute for Surface and Interface Science, University of California, Irvine, CA 92697, USA

ARTICLE INFO

Article history:
Received 20 August 2010
Received in revised form 4 December 2010
Accepted 11 January 2011
Available online 21 January 2011

Keywords:
Scattering
Anisotropy
Two-dimensional randomly rough surfaces
Perfect conductor
Rigorous computer simulations

ABSTRACT

An approach is introduced for performing rigorous numerical simulations of electromagnetic wave scattering from randomly rough, perfectly conducting surfaces. It is based on a surface integral technique, and consists of determining the unknown electric surface current densities from which the electromagnetic field everywhere can be determined. The method is used to study the scattering of a *p*-polarized beam from an *anisotropic* Gaussian, randomly rough, perfectly conducting surface. It is demonstrated that the surface anisotropy gives rise to interesting and pronounced signatures in the angular intensity distribution of the scattered light. The origins of these features are discussed.

1. Introduction

Theoretical/computational studies of the scattering of light from two-dimensional randomly rough perfectly conducting surfaces are carried out primarily for two reasons. These are that a perfectly conducting surface is a good approximation to a finitely conducting surface in the far infrared region of the optical spectrum, but computationally less intensive to study than a finitely conducting surface, and that the development of computational methods for calculations of scattering from rough perfectly conducting surfaces can serve as the first step in the development of methods that can be used in calculations of scattering from rough finitely conducting surfaces.

The existing studies of the scattering of light from two-dimensional randomly rough perfectly conducting surfaces by rigorous methods [1–7] have been based on the assumption that the surface profile function $\zeta(\mathbf{x}_\parallel)$, where $\mathbf{x}_\parallel = (x_1, x_2, 0)$, that defines the position of the surface by $x_3 = \zeta(\mathbf{x}_\parallel)$ is a stationary zero-mean, *isotropic*, Gaussian random process. Very little work has been devoted to the case where $\zeta(\mathbf{x}_\parallel)$ is an *anisotropic* random process. In this paper we present results, obtained by a rigorous computational approach, for the electromagnetic field scattered from a two-dimensional, random, perfectly conducting surface defined by a surface profile function that is a stationary, zero-mean, anisotropic, Gaussian random process.

2. The scattering system

The scattering system that we consider in this work is illustrated in Fig. 1. It consists of vacuum in the region $x_3 > \zeta(\mathbf{x}_\parallel)$, and a perfect conductor in the region $x_3 < \zeta(\mathbf{x}_\parallel)$. The surface profile function $\zeta(\mathbf{x}_\parallel)$ is assumed to be a single-valued function of $\mathbf{x}_\parallel$ that is differentiable with respect to x_1 and x_2, and constitutes a stationary, zero-mean, Gaussian random process defined by

$$\langle \zeta(\mathbf{x}_\parallel) \rangle = 0, \tag{1}$$

$$\langle \zeta(\mathbf{x}_\parallel) \zeta(\mathbf{x}'_\parallel) \rangle = \delta^2 W(\mathbf{x}_\parallel - \mathbf{x}'_\parallel), \tag{2}$$

where $\delta = \sqrt{\langle \zeta^2(\mathbf{x}_\parallel) \rangle}$ is the root-mean-square (rms) roughness of the surface, and $W(\mathbf{x}_\parallel)$ is the surface height auto-correlation function that is normalized so that $W(\mathbf{0}) = 1$, and vanishes as $|\mathbf{x}_\parallel| \to \infty$. In Eqs. (1) and (2) the angle brackets denote an average over the ensemble of realizations of the surface profile function. It should be noted from Eq. (2) that the correlation function $W(\cdot)$ depends on *both* the direction and length of its argument. Thus, in contrast to what has been assumed in the majority of previous studies of rough surface scattering, the surface here may potentially be *anisotropic*. The power spectrum of the surface roughness is defined by

$$g(\mathbf{k}_\parallel) = \int d^2 x_\parallel W(\mathbf{x}_\parallel) \exp(-i\mathbf{k}_\parallel \cdot \mathbf{x}_\parallel). \tag{3}$$

* Corresponding author at: Department of Physics, Norwegian University of Science and Technology (NTNU), NO-7491 Trondheim, Norway.
E-mail addresses: Ingve.Simonsen@phys.ntnu.no (I. Simonsen), aamaradu@uci.edu (A.A. Maradudin), tleskova@uci.edu (T.A. Leskova).

0010-4655/$ – see front matter
doi:10.1016/j.cpc.2011.01.010

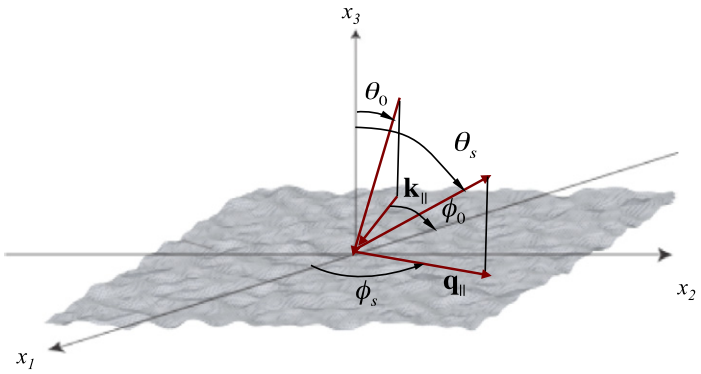

Fig. 1. Illustration of the scattering geometry considered in the present work, where the coordinate system used and angles of incidence (θ_0, ϕ_0) and scattering (θ_s, ϕ_s) are defined.

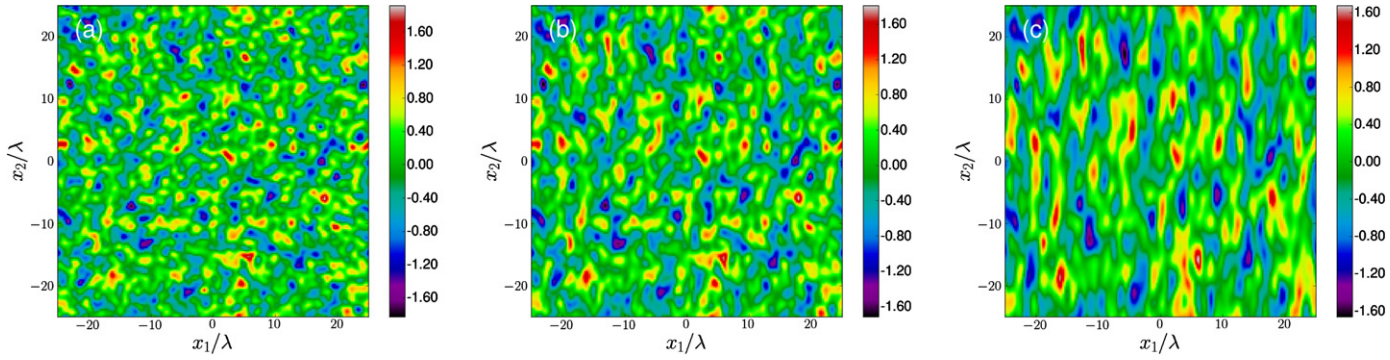

Fig. 2. A segment of one numerically generated realization of each of the three different types of surfaces used in the numerical calculations of this paper. The surfaces are characterized by a Gaussian height distribution of rms-value $\delta = \lambda/2$, where λ is the wavelength of the incident light, and a Gaussian correlation function of transverse correlation lengths $a_1 = \lambda$ and: (a) $a_2 = \lambda$, the isotropic case; (b) $a_2 = 1.5\lambda$, the weakly anisotropic case; and (c) $a_2 = 3\lambda$, the strongly anisotropic case. The same underlying random numbers $(X_{m,n})$ were used to generate each of these surfaces. The scale of the contour plots corresponds to $\zeta(\mathbf{x}_\parallel)/\lambda$.

In the numerical calculations to be carried out in this work, we will assume an anisotropic Gaussian form for the surface height auto-correlation function. Without loss of generality, the two directions corresponding to the directions of shortest and longest correlation lengths will be chosen to coincide with the x_1 and x_2 axes of the coordinate system [Fig. 1], respectively. Under this assumption, an anisotropic Gaussian correlation function can be defined as

$$W(\mathbf{x}_\parallel) = \exp\left[-\frac{x_1^2}{a_1^2} - \frac{x_2^2}{a_2^2}\right], \tag{4}$$

where a_1 and a_2 are the correlation lengths for the x_1 and x_2 directions, respectively, and it is assumed that $a_1 \leqslant a_2$. For this reason (with our convention), we will refer to the x_1 and x_2 axes as the minor and major axes of the anisotropy, respectively. When $a_1 = a_2 \equiv a$ the surface is isotropic and the correlation function (4) reduces to the more familiar isotropic Gaussian form, $\exp[-x_\parallel^2/a^2]$, that depends only on the length (and not the direction) of the spatial argument $\mathbf{x}_\parallel$ [8]. For the correlation function Eq. (4), the corresponding power-spectrum reads

$$g(\mathbf{k}_\parallel) = \pi a_1 a_2 \exp\left[-\frac{k_1^2 a_1^2}{4} - \frac{k_2^2 a_2^2}{4}\right], \tag{5}$$

and is elongated along the minor axis of the anisotropy.

An ensemble of randomly rough surfaces of such statistical properties can be generated numerically by the so-called Fourier filtering method [9]. In this method we first define a two-dimensional square lattice of points by $\mathbf{x}(m,n) = (m,n,0)\Delta x$ with $m,n = 0, \pm 1, \pm 2, \ldots$. With each site (m,n) of this lattice we associate an independent, zero-mean, Gaussian random deviate $X_{m,n}$ with a standard deviation of unity, so that $\langle X_{m,n}\rangle = 0$ and $\langle X_{m,n} X_{m',n'}\rangle = \delta_{mm'}\delta_{nn'}$. The surface profile function at the point $\mathbf{x}_\parallel = \mathbf{x}(m,n)$ is then written in the form

$$\zeta\big(\mathbf{x}(m,n)\big) = \delta \sum_{k,l} W_{k,l} X_{k+m,l+n}\,, \tag{6}$$

where the $\{W_{k,l}\}$ are real weights to be determined. The surface height auto-correlation function then takes the form

$$\begin{aligned}\big\langle \zeta\big(\mathbf{x}(m,n)\big)\zeta\big(\mathbf{x}(m+i,n+j)\big)\big\rangle &= \delta^2 \sum_{k,l} W_{k,l} W_{k-i,l-j} \\ &= \delta^2 \int \frac{d^2 Q_\parallel}{(2\pi)^2} g(\mathbf{Q}_\parallel) \exp\big[i\mathbf{Q}_\parallel \cdot \mathbf{x}(i,j)\big],\end{aligned} \tag{7}$$

where Eq. (2) and the inverse of Eq. (3) were used in obtaining this result. We now introduce the representation $W_{m,n} = \int \frac{d^2 P_\parallel}{(2\pi)^2} \widehat{W}(\mathbf{P}_\parallel) \exp[i\mathbf{P}_\parallel \cdot \mathbf{x}(m,n)]$, and find from Eq. (7) that $\widehat{W}(\mathbf{Q}_\parallel) = \Delta x\, g^{1/2}(\mathbf{Q}_\parallel)$, so that finally

$$W_{m,n} = \int \frac{d^2 Q_\parallel}{(2\pi)^2} g^{1/2}(\mathbf{Q}_\parallel) \exp\big[i\mathbf{Q}_\parallel \cdot \mathbf{x}(m,n)\big]. \tag{8}$$

From this result and Eq. (6) an ensemble of randomly rough surfaces was generated and used in the numerical calculations; see Fig. 2.

3. Formulation

The solution of the scattering problem, is obtained by solving the Maxwell equations with the proper boundary conditions on

the rough surface as well as at infinity. For our purposes, however, it is more convenient to base the formulation on the Stratton–Chu formulas [10] for the magnetic field $\mathbf{H}(\mathbf{x}_\parallel|\omega)$, in the vacuum region above the perfectly conducting surface,

$$\mathbf{H}(\mathbf{x}_\parallel|\omega)_{inc} + \frac{1}{4\pi}\int d^2x'_\parallel \left[\nabla' g_0\left(\mathbf{x}|\mathbf{x}'\right)\right]\Big|_{x'_3=\zeta(\mathbf{x}'_\parallel)} \times \mathbf{J}_H\left(\mathbf{x}'_\parallel|\omega\right) = \theta\left(x_3-\zeta(\mathbf{x}_\parallel)\right)\mathbf{H}(\mathbf{x}_\parallel|\omega). \quad (9)$$

Here the function $g_0(\mathbf{x}|\mathbf{x}') = \exp[i(\omega/c)|\mathbf{x}-\mathbf{x}'|]/|\mathbf{x}-\mathbf{x}'|$ is the scalar free-space Green's function, where ω and c are the angular frequency and speed of light in vacuum, respectively, and $\theta(\cdot)$ denotes the Heaviside unit step function. For all fields a time-harmonic dependence $\exp(-i\omega t)$ was assumed, but not indicated explicitly. Moreover, in writing Eq. (9) an (electric) surface current density has been defined as

$$\mathbf{J}_H(\mathbf{x}_\parallel|\omega) = \left[\mathbf{n}\times\mathbf{H}(\mathbf{x}|\omega)\right]\Big|_{x_3=\zeta(\mathbf{x}_\parallel)}, \quad (10)$$

where $\mathbf{n} = (-\partial\zeta(\mathbf{x}_\parallel)/\partial x_1, -\partial\zeta(\mathbf{x}_\parallel)/\partial x_2, 1)$ is a vector that is normal to the surface $x_3 = \zeta(\mathbf{x}_\parallel)$ at each point and is directed into the vacuum.

We note that Eq. (9) determines the magnetic field *everywhere* in the region above the rough surface, and that the electric field is obtained directly from the magnetic *via* Ampere's law. Therefore, the solution of the scattering problem is reduced to determining the unknown surface current $\mathbf{J}_H(\mathbf{x}_\parallel|\omega)$.

This is done most readily by deriving and solving an integral equation for $\mathbf{J}_H(\mathbf{x}_\parallel|\omega)$. Such an equation can be obtained by evaluating the Stratton–Chu formula (9) infinitesimally above and below the surface $x_3 = \zeta(\mathbf{x}_\parallel)$, adding the resulting equations, and taking the vector cross product of $\mathbf{n}$ with the sum. By this procedure, one is led to the following integral equation satisfied by the surface current

$$\mathbf{J}_H(\mathbf{x}_\parallel|\omega) + \frac{1}{2\pi}P\int d^2x'_\parallel\, \mathbf{n}\times\left\{\left[\!\left[\nabla g_0\left(\mathbf{x}|\mathbf{x}'\right)\right]\!\right]\times\mathbf{J}_H\left(\mathbf{x}'_\parallel|\omega\right)\right\} = 2\mathbf{J}_H^{(i)}(\mathbf{x}_\parallel|\omega), \quad (11)$$

where the relation $\nabla' g_0(\mathbf{x}|\mathbf{x}') = -\nabla g_0(\mathbf{x}|\mathbf{x}')$ has also been used. In writing Eq. (11), $\mathbf{J}_H^{(i)}(\mathbf{x}_\parallel|\omega)$ was defined similarly to Eq. (10) but in terms of the incident field $\mathbf{H}(\mathbf{x}|\omega)_{inc}$; P denotes the Cauchy principal part of the integral; and the compact "double bracket" notation is defined as

$$\left[\!\left[f\left(\mathbf{x}|\mathbf{x}'\right)\right]\!\right] = f\left(\mathbf{x}|\mathbf{x}'\right)\Big|_{\substack{x_3=\zeta(\mathbf{x}_\parallel)\\ x'_3=\zeta(\mathbf{x}'_\parallel)}}. \quad (12)$$

Eq. (11) represents a set of three coupled integral equations for the three components of $\mathbf{J}_H(\mathbf{x}_\parallel|\omega)$. However, owing to the fact that $\mathbf{n}\cdot\mathbf{J}_H(\mathbf{x}_\parallel|\omega) = 0$, only two of these components are independent, and $\mathbf{J}_H(\mathbf{x}_\parallel|\omega)_3$, say, may be eliminated leaving only two coupled inhomogeneous integral equations [7]. The resulting set of two coupled integral equations for $\mathbf{J}_H(\mathbf{x}_\parallel|\omega)_{1,2}$ is solved by converting it into a pair of coupled matrix equations. This is done by generating a realization of the surface profile function on a grid of N^2 points within a square region of the x_1x_2 plane of edge L, where the ratio $L/N = \Delta x$ is chosen to be $\Delta x = \lambda/7$, with λ the wavelength of the incident field. If both the integral kernel and the unknown surface currents are assumed to vary slowly over an area $(\Delta x)^2$ centered around the point $(x_1, x_2, 0)$, the integral equation (11) is readily converted into a complex dense matrix system by the extended mid-point method [11]. The principal value integral ensures that there is no divergence caused by the derivatives of the Green's function at $\mathbf{x}_\parallel = \mathbf{x}'_\parallel$. The memory footprint of the matrix system scales like $4N^4$, so preferably one should use iterative methods to solve it if such methods converge for the level of roughness that one is interested in. In this work we have used the biconjugate gradient stabilized (BiGCStab) method [12] for this purpose. Once the matrix system is solved and the equation $\mathbf{n}\cdot\mathbf{J}_H = 0$ used to calculate $\mathbf{J}_H(\mathbf{x}_\parallel|\omega)_3$ from it, the magnetic component of the electromagnetic field can be obtained from Eq. (9). The corresponding electric field is obtained from the magnetic field *via* Ampere's law.

The physical quantity that we will be concerned with is the mean differential reflection coefficient, $\langle\partial R_{\nu_s,\nu_0}/\partial\Omega_s\rangle$, for the scattering of linearly ν_0-polarized incident light into linearly ν_s-polarized scattered light. The differential reflection coefficient is defined such that $\langle\partial R_{\nu_s,\nu_0}/\partial\Omega_s\rangle d\Omega_s$ is the fraction of the total time-averaged flux incident on the surface that is scattered into the element of solid angle $d\Omega_s$ about the scattering direction (θ_s, ϕ_s) [7]. Since we are concerned with scattering from a randomly rough surface, it is the average of this quantity over an ensemble of realizations of the surface that we need to calculate, and it can be expressed in terms of the surface currents (see Ref. [7] for details). Since a perfectly conducting surface has no absorption or transmission, all energy that is incident on it has to be scattered back into the medium of incidence. Hence, energy conservation requires that the integral over all possible scattering directions of the mean differential reflection coefficient should be one. This can be used to estimate the consistency and quality of the numerical calculations. For all the numerical simulation results to be presented in this work, energy conservation was explicitly checked and found to be satisfied with an error of less than 0.4%.

4. Results and discussions

By the approach outlined in the preceding section, we have performed rigorous computer simulations for the scattering of p-polarized incident light from randomly rough, perfectly conducting surfaces characterized by a Gaussian height distribution of rms-value $\delta = \lambda/2$ and a Gaussian correlation function with correlation lengths $a_1 = \lambda$ and either (i) $a_2 = \lambda$ (isotropic surface; Fig. 3); (ii) $a_2 = 1.5\lambda$ (weakly anisotropic surface; Fig. 4); or (iii) $a_2 = 3\lambda$ (strongly anisotropic surface Fig. 5). For all these cases the p-polarized light was incident at angles $(\theta_0, \phi_0) = (20^\circ, 45^\circ)$.

For later comparison, we start by considering an isotropic system for which the full angular distributions of the mean differential reflection coefficients are presented in Fig. 3. A similar system has recently been discussed in the literature [7], and the interested reader is referred to that publication for additional details about the scattering properties of isotropic random surfaces. We note from Fig. 3, or from Ref. [7], that the co-polarized ($p \to p$) scattering consists of a dipole-like angular distribution with the main intensity oriented *parallel* to the plane of incidence [Fig. 3(b)]. In contrast, for cross-polarization ($p \to s$) the main intensity distribution is oriented *perpendicular* to the plane of incidence [Fig. 3(c)]. For both cases (if the surface is isotropic), the intensity distributions are symmetric with respect to the plane of incidence, and the intensity distributions of the scattered light are independent of the azimuthal angle of incidence, ϕ_0, except for a trivial rotation of the scattered intensity patterns. When the polarization of the scattered light is not recorded [Fig. 3(a)], the dipole-like angular distributions that were seen for both co- and cross-polarized scattering are not easily observed. In passing we note that the pronounced peak in the backscattering direction ($\theta_s = \theta_0$ and $\phi_s = \phi_0 + 180^\circ$) is an enhanced backscattering peak, which finds its physical origin in multiple scattering [13].

When the randomly rough surface is anisotropic, the angular distribution of the scattered light is more complex than that for the corresponding isotropic geometry. For instance, the intensity of the scattered light from an anisotropic surface will in general *not* be symmetric about the plane of incidence. However, even

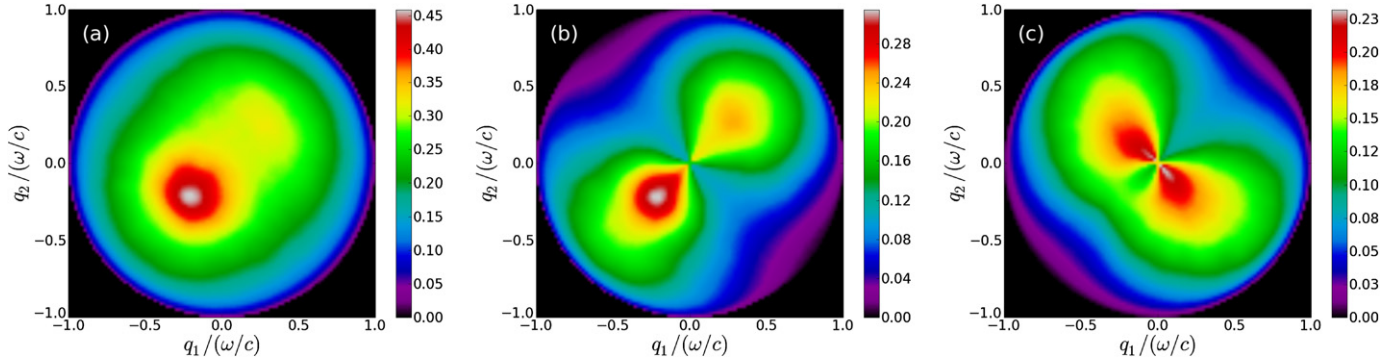

Fig. 3. A p-polarized beam of wavelength λ and width $w = 4\lambda$ is scattered from an *isotropic* perfectly conducing rough surface characterized by a Gaussian height distribution of rms-value $\delta = \lambda/2$ and a Gaussian correlation function of correlation lengths $a_1 = a_2 = \lambda$. The panels show contour plots of the full angular distributions of the mean differential reflection coefficient, $\langle \partial R_{\nu_s,p}/\partial \Omega_s \rangle$, obtained by a rigorous computer simulation approach for the scattering of the beam incident on the rough surface at a polar angle $\theta_0 = 20^\circ$ and an azimuthal angle $\phi_0 = 45^\circ$. The three panels correspond to various configurations for the polarization of the scattered light. They are: (a) the polarization of the scattered light is not recorded [$\nu_s = p, s$]; (b) only p-polarized scattered light is measured [$\nu_s = p$]; and (c) only s-polarized scattered light is recorded [$\nu_s = s$]. The rough surface, covering an area $16\lambda \times 16\lambda$, was discretized on a grid of 112×112 points corresponding to a discretization interval $\lambda/7$ for both directions. The presented figures were obtained by averaging the mean differential reflection coefficient over results for 6000 surface realizations.

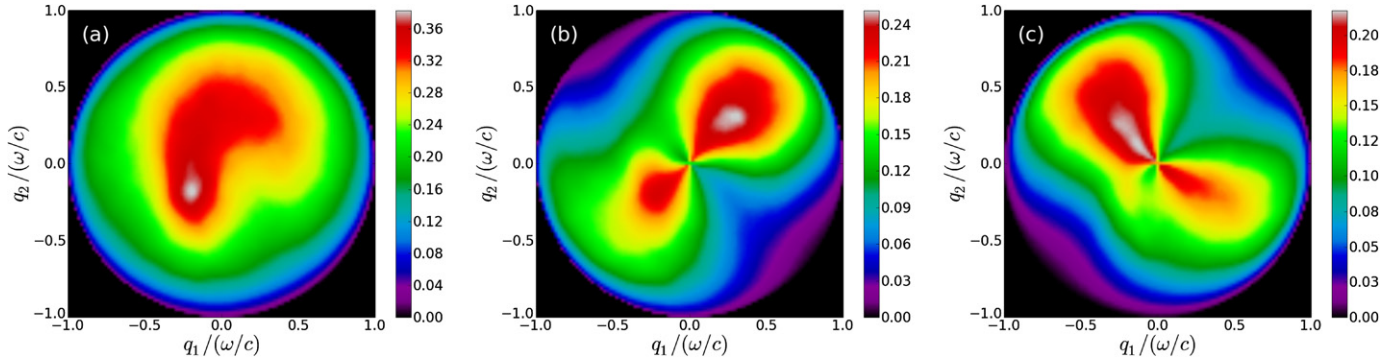

Fig. 4. Same as Fig. 3 with the only difference being that the surface now is *weakly anisotropic* and characterized by the correlation lengths $a_1 = \lambda$ and $a_2 = 1.5\lambda$.

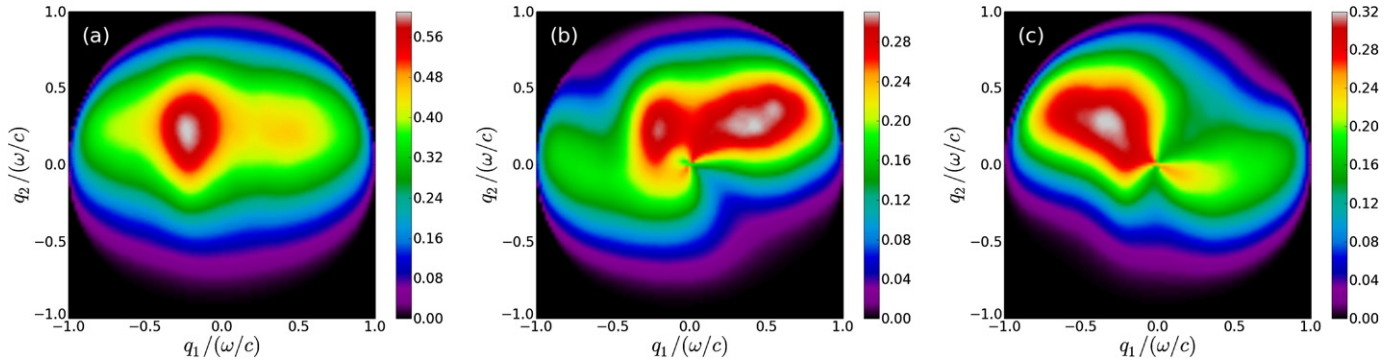

Fig. 5. Same as Fig. 3 with the only difference being that the surface now is *strongly anisotropic* and characterized by the correlation lengths $a_1 = \lambda$ and $a_2 = 3\lambda$.

in the anisotropic case, it has been found (see discussion below) that the intensity distributions are symmetric about the plane of incidence whenever the projection of the incident wave vector onto the mean plane, $\mathbf{k}_\parallel = (\omega/c)(\sin\theta_0 \cos\phi_0, \sin\theta_0 \sin\phi_0, 0)$, is parallel to either the minor or the major axis of the anisotropy [$\phi_0 \in [0^\circ, \pm 90^\circ, 180^\circ]$]. For such cases the angular intensity distributions of the scattered light are qualitatively rather similar to those shown in Fig. 3 for the isotropic case. This conclusion holds for both co- and cross-polarized scattering as well as when the polarization of the scattered light is not recorded.

However, the main difference between the angular intensity distributions of the light scattered from isotropic and anisotropic surfaces can be observed when the azimuthal angle of incidence, ϕ_0, is such that $\mathbf{k}_\parallel$ is neither parallel to the minor nor to the major axis of the anisotropy. One particular such situation is considered in Fig. 4 for which the azimuthal angle of incidence was $\phi_0 = 45^\circ$ and the correlation lengths of the anisotropic random surface were $a_1 = \lambda$ and $a_2 = 1.5\lambda$ [see Fig. 2(b)]. By comparing the scattering from the isotropic [Fig. 3(a)] and the related anisotropic surface [Fig. 4(a)] for the case when the polarization of the scattered light was not recorded, it is observed that what is a well-defined enhanced backscattering peak in the case of the isotropic surface, becomes a much broader "bandy stick" shaped region of high intensity that includes the backscattering direction for the anisotropic surface. This latter high-intensity structure is predominantly oriented along the major axis of the anisotropy, and the bandy stick blade is directed towards the specular direction in the forward scattering plane [Fig. 4(a)]. It is noted that a peak is still visible in Fig. 4(a) in the backscattering direction, but it seems to be less intense. In order to interpret this result,

it is instructive to study in some more detail the angular distribution of the mean differential reflection coefficients in the co- and cross-polarized configurations, Figs. 4(b)–(c), and to compare them to the corresponding figures for the isotropic counterparts. Figs. 4(b)–(c) show explicitly that the dipole-like angular scattering patterns lack the symmetry with respect to the plane of incidence that the isotropic equivalents have. This asymmetry of the angular distribution of the scattered intensity expresses itself as a larger fraction of the intensity incident on the surface being scattered to one side of the incident plane relative to the other. From the computer simulation results for weakly anisotropic surfaces depicted in Figs. 4(b)–(c), this asymmetry is particularly apparent in the cross-polarized scattering. The cross-polarized component of the mean differential reflection coefficient is to lowest (single scattering) order proportional to $g(\mathbf{q}_\parallel - \mathbf{k}_\parallel)[(\hat{\mathbf{q}}_\parallel \times \hat{\mathbf{k}}_\parallel) \cdot \hat{\mathbf{x}}_3]^2$, where $\mathbf{q}_\parallel = (\omega/c)(\sin\theta_s \cos\phi_s, \sin\theta_s \sin\phi_s, 0)$ [14]. For anisotropic surfaces, this function is not symmetric with respect to the plane of incidence, and the trend in its angular dependence is consistent with what is observed in Fig. 4(c).

The co-polarized scattering pattern is explained in a similar way. In this case, the single scattering contribution to the co-polarized component of the mean differential reflection coefficient contains terms of the form $g(\mathbf{q}_\parallel - \mathbf{k}_\parallel)[\hat{\mathbf{q}}_\parallel \cdot \hat{\mathbf{k}}_\parallel]^m$, with $m = 1, 2$. The positions of the maxima of such functions are in the forward direction and, when the surface is anisotropic, they move away from the plane of incidence and toward the minor axis of the anisotropy [Fig. 4(b)].

When the surface becomes strongly anisotropic [Fig. 2(c)], most of the features of the weakly anisotropic surfaces discussed above seem to hold, only becoming more pronounced. For instance, in Fig. 5(a) high scattered intensity at the position $(\theta_s, \phi_s) \approx (\theta_0, 180^\circ - \phi_0)$ is readily seen, and is due to cross-polarized scattered light, as was explained for the weakly anisotropic case. The cross-polarized contribution to the scattered light is seen in Fig. 5(c). However, the co-polarized component of the mean differential reflection coefficient seems to be somewhat different for the strongly anisotropic case [Fig. 5(b)]. The reason for this is to be found in an additional term in the single scattering contribution to $\langle \partial R_{pp}/\partial \Omega_s \rangle$. This term is proportional to $g(\mathbf{q}_\parallel - \mathbf{k}_\parallel)$, and does not have any additional ϕ_0 or ϕ_s dependence. Hence, as the surface becomes strongly anisotropic, and the power-spectrum decays rapidly along the major axis of the anisotropy, this term will start playing a more and more important role, resulting in a pattern elongated along the minor axis of the anisotropy.

5. Conclusions

We have introduced a reliable numerical simulation approach capable of producing rigorous results for the scattering of light, both co- and cross-polarized, from two-dimensional, randomly rough, perfectly conducting surfaces. By this method we study the scattering of a *p*-polarized beam from an *anisotropic* Gaussian, randomly rough, perfectly conducting surface. It is demonstrated that the surface anisotropy gives rise to interesting and pronounced signatures in the angular intensity distribution of the scattered light.

Acknowledgements

This research was supported in part by AFRL contract FA9453-08-C-0230.

References

[1] P. Tran, V. Celli, A.A. Maradudin, J. Opt. Soc. Am. A 11 (1994) 1686.
[2] R.L. Wagner, J. Song, W.C. Chew, IEEE Trans. Antennas Propag. 45 (1997) 235.
[3] K. Pak, L. Tsang, C.H. Chan, J.T. Johnson, J. Opt. Soc. Am. A 12 (1995) 2491.
[4] J.T. Johnson, L. Tsang, R.T. Shin, K. Pak, C.H. Chan, A. Ishimaru, Y. Kuga, IEEE Trans. Antennas Propag. 44 (1996) 748.
[5] D. Torrungrueng, H.-T. Chou, J.T. Johnson, IEEE Trans. Geosci. Remote Sensing 38 (2000) 1656.
[6] G. Soriano, M. Saillard, J. Opt. Soc. Am. A 18 (2001) 124.
[7] I. Simonsen, A.A. Maradudin, T.A. Leskova, Phys. Rev. A 81 (2010) 013806.
[8] H.E. Bennett, J.O. Porteus, J. Opt. Soc. Am. A 2 (1985) 2285.
[9] J.D. Rochier, A.J. Blanchard, M.F. Chen, Int. J. Remote Sensing 10 (1989) 1155.
[10] J.A. Kong, Electromagnetic Wave Theory, EMW Publishing, Cambridge, MA, 2005, pp. 674–675.
[11] W.H. Press, S.A. Teukolsky, W.T. Vetterling, B.P. Flannery, Numerical Recipes in Fortran, 2nd ed., Cambridge University Press, New York, 1992, p. 129.
[12] H. van der Vorst, SIAM J. Sci. Statist. Comput. 13 (1992) 631.
[13] K.A. O'Donnell, E.R. Méndez, J. Opt. Soc. Am. A 4 (1987) 1194.
[14] A.R. McGurn, A.A. Maradudin, Waves Random Media 6 (1996) 251.